PROCEEDINGS, 45th Workshop on Geothermal Reservoir Engineering
Stanford University, Stanford, California, February 10-12, 2020
SGP-TR-216

Pumping Tests and Hydraulic Tomography in Fractured Granite, Blair Wallis, Laramie Range, Wyoming

Shuangpo Ren[1], Ye Zhang[2], Yuli Wang[3], Tian-Chyi Jim Yeh[3], Bradley J. Carr[2]

[1]Key Laboratory of Tectonics and Petroleum Resources, China University of Geosciences, Ministry of Education, Wuhan 430074, PR China

[2]Department of Geology and Geophysics, University of Wyoming, Laramie, WY, USA

[3]Department of Hydrology and Atmospheric Science, University of Arizona, Tucson, AZ, USA

yzhang9@uwyo.edu

Keywords: fractured granite, hydraulic conductivity, storativity, hydraulic tomography, cross-hole well test

ABSTRACT

We investigated the hydraulic properties of a fractured granite aquifer in the Laramie Range, Wyoming, using cross-hole pumping tests among six boreholes ranging from 16-76 m deep. Results of four cross-hole pumping tests were interpreted using analytical conceptual models and using SimSLE, a two-dimensional transient hydraulic tomography (HT) algorithm (Xiang et al., 2009). A set of field-scale vertically averaged horizontal hydraulic conductivities (Kh) was interpreted first using analytical models, i.e., Theis (1935), Cooper and Jacob (1946), Neuman (1974), and Moench (1997). The estimated Kh values are very close despite the difference in the assumptions of these analytical models. HT is a useful technique for imaging inter-well permeability heterogeneity. The SimSLE algorithm was able to image, between these boreholes, continuous high Kh and low specific storage (Ss) zones, thus areas with high hydraulic diffusivity. These inter-well zones allow fast preferential flows that reflect connectivity of fractures between the boreholes. In addition, the same algorithm identified a low Kh barrier between one borehole and the rest of the well field, which is consistent with what is known from site geological, drilling, and geophysical data. Finally, scale effect is observed as the pumping-test-inferred Kh is more than a factor of 5 greater than the slug-test-inferred Kh for several boreholes, suggesting fractures with greater permeability were encountered when the well test volume was expanded.

1. INTRODUCTION

In groundwater hydrology, hydraulic tomography (HT) is a relative new inverse method for obtaining detailed spatial distributions of inter-well hydraulic parameters such as hydraulic conductivity (K) and storativity. To perform a HT experiment, a series of cross-hole pumping (or injection) tests are performed sequentially on wells or boreholes completed in a given geological formation. According to Illman (2014), hydraulic tomography was first proposed by Neuman (1987), who considered it to be an analog of geophysical tomography. After that, considerable effort has been made to develop new and improved algorithms to implement HT (Yeh et al., 1996; Snodgrass and Kitanidis, 1998; Yeh and Liu, 2000; Zhu and Yeh 2005; Castagna and Bellin, 2009; Xiang et al., 2009; Liu and Kitanidis, 2011; Schöniger et al., 2012). Yeh et al. (1996) developed an iterative geostatistical technique, referred to as the successive linear estimator (SLE), which jointly interprets steady-state hydraulic head measurements from a hydraulic tomography experiment. Compared to conventional geostatistical techniques such as cokriging, SLE can reveal more spatial details on the parameters. Moreover, the flow physics, as embodied in the groundwater flow equation solved by SLE, is honored while most cokriging methods do not condition the parameters on dynamic data. Based on the SLE method, Sequential SLE (SSLE) and Simultaneous SLE (SimSLE) were also developed which take advantage of transient hydraulic head measurements (Yeh and Liu, 2000; Zhu and Yeh, 2005; Xiang et al., 2009). SimSLE interprets transient hydraulic head observations simultaneously and has several advantages over the SSLE (Xiang et al., 2009). In recent years, joint inversion of hydraulic data with tracer measurements have also been developed by extending the HT techniques to include the inversion of solute concentration data (Jardani et al., 2013).

For unconsolidated porous media, the efficacy of HT has been demonstrated in numerical experiments (e.g., Zhu and Yeh, 2005), laboratory experiments (e.g., Liu et al., 2002), and field studies (e.g., Cardiff et al., 2012; Berg and Illman, 2013). However, the application of HT to the hydraulic characterization of hard rock aquifers, in particular, fractured rocks, is still limited. Hao et al. (2008) investigated the ability of SSLE to identify fracture zones as well as their connectivity in two dimensions using a synthetic fractured medium. These authors demonstrated that as the number of boreholes and monitoring ports increased, the recovery of the fracture pattern and their connectivity became more accurate while estimation uncertainty was reduced. Using numerical experiments, Castagna et al. (2011) also performed a 2D HT inversion for fractured rocks. Their results indicated that the accuracy of the estimated transmissivity and storativity fields are highly dependent on the spatial structure of the storativity. Similarly, using numerical experiments simulating pumping tests in a confined aquifer, Sharmeen et al. (2012) conducted transient HT to image both the K and specific storage (Ss) tomograms of fractured rocks. Fracture locations and geometry were unknown in their inversion analysis. Results suggested that the transient HT technique can effectively depict the high K and low Ss zones that nearly coincided with the location of the fractures as well as their intersections.

The study performed by Meier et al. (2001) was the first known HT experiment at a field site where a number of wells were completed in fractured granite. In their study, multiple cross-hole hydraulic tests were simultaneously analyzed in two dimensions to reveal the main fracture pattern at the site. More recently, Illman et al. (2009) analyzed two cross-hole pumping tests using the SSLE algorithm at the Mizunami Underground (MIU) Research Laboratory construction site in central Japan. Three-dimensional distribution of K and Ss, as well as their uncertainty, were obtained. These authors also evaluated fracture connectivity at the site, which controls large-scale groundwater flow in crystalline rocks. Zha et al. (2016) extended Illman et al. (2009)'s work by adding field measurements from two new pumping tests at MIU to the HT interpretation. As expected, their results provided improved imaging of fracture and fault zones at the kilometer scale. Castagna et al (2011) analyzed five cross-hole pumping tests to obtain both transmissivity and storativity tomograms of a quartzose sandstone that contains a single sub-horizontal fracture at the Altona Flat Rock site, New York. The authors found that the estimated storativity appeared to be more heterogeneous than it is typically assumed. Their results suggested that heterogeneity in both transmissivity and storativity should be accounted for when hydraulic tomography was used to interpret field data.

In this work, we performed a series of cross-hole pumping tests in a fractured granite aquifer at the Blair Wallis Fractured Rock Hydrology Research Well Field in the Laramie Range in southeastern Wyoming. The goal of our study is to characterize hydraulic parameters and their corresponding uncertainty estimates at various scales using classic well test interpretation and hydraulic tomography. The HT survey was performed among six bedrock wells (BW1-BW9) with open-hole completion, thus the measured hydraulic heads reflect vertically averaged head in the fractured aquifer. Accordingly, vertically averaged horizontal hydraulic conductivity (Kh) and specific storage (Ss) were estimated by HT, which can be compared to classic well-test interpretation using single- and cross-hole analytical solutions assuming homogeneous parameters. Using the SimSLE algorithm, transient drawdown data from sequential pumping tests were jointly inverted to obtain images of (vertically averaged) Kh and specific storage (Ss) among the boreholes. From the images, several high-Kh and low-Ss zones can be distinguished at the well field, while the algorithm further identified a low conductivity zones between BW4 and the rest of the well field indicating the existence of a low-permeability barrier. This HT-inferred flow barrier is consistent with independent site geological, geophysical, and drilling data.

2. FIELD SITE

The Blair Wallis Fractured Rock Hydrology Research Well Field lies within the semi-arid Crow Creek Watershed of the Laramie Range which lies within US Forest Service land about 21 km southeast of Laramie, Wyoming (Figure 1). The Laramie Range, extending from the Colorado-Wyoming border to the Powder River basin in southeastern Wyoming, consists of Precambrian crystalline rocks that was uplifted over sedimentary Phanerozoic-aged rocks during the Laramide Orogeny (Johnson and Hills, 1976). Previous studies indicate that the Blair Wallis well field is part of the Rocky Mountain surface (Bradley, 1987; Chapin and Kelley, 1997; Eggler et al., 1969; Evanoff, 1990) that originated from the Eocene (Gregory and Chase, 1994; Mears, 1993; Moore, 1960; Scott and Taylor, 1986). In this well field, which lies in a cold and exposed hillslope in the Laramie Range, approximately 5~15 m of weathered granitic soil (i.e., saprolite) overlies granite bedrock that is the focus of this investigation. The granite bedrock is highly fractured, to the extent that the northern portion of the Laramie Range may have rotated southward (Blackstone, 1996). This is confirmed by geologic mapping studies that identified numerous surficial lineaments in the region (Ochsner, 2014). At the Blair Wallis well field, depth-to-water varies from ~5 to 15 m below ground source, and the water table generally lies within the granite bedrock and follows the topographic gradient. The bedrock aquifer is unconfined, although individual fractures may be confined or become unconfined when the water table drops. Hydraulic tests at the well field, as explained below, confirmed that many bedrock fractures are open, allowing water storage and transmission at the km scale.

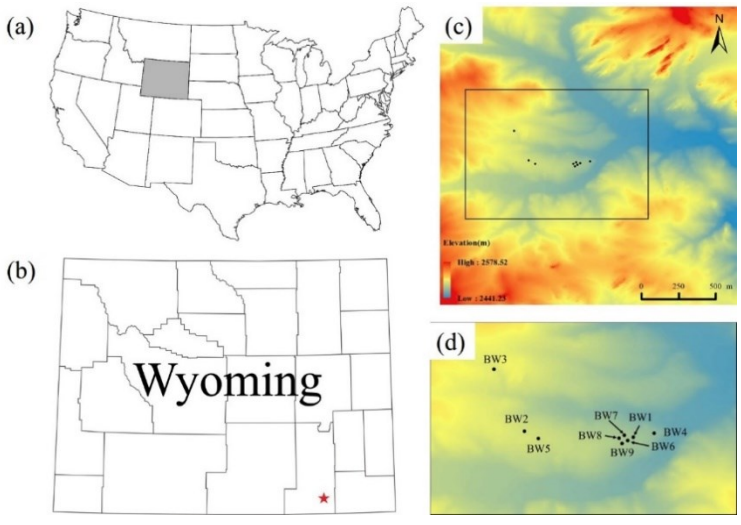

Figure 1 Location of the Blair Wallis Fractured Rock research well field. (a) Location of Wyoming in the USA, (b) Location of the well field in Wyoming (shown as a red star), (c) Elevation of the well field extracted from light detecting and ranging (LIDAR) elevation data, and (d) A zoom-in view of the nine granite well locations.

At the Blair Wallis well field, nine wells have been completed in the granite bedrock: all wells are cased ~5 feet below the bottom of the saprolite but remain open boreholes in the underlying fractured granite. After casing was set at each borehole, cores were recovered using a rotary drill from BW1, BW2, BW3, BW4, and BW5. Cores, however, were not recovered from BW6-9. The cores were photographed using a Geotek core logger with a Sigma 105-mm microlens, which identified fractures in both sub-vertical and sub-horizontal to horizontal directions. For a subset of the boreholes, a Mount Sopris QL40-OBI-2G Optical Televiewer (Mt. Sopris Instruments, Denver, CO) was deployed to provide 360° unwrapped optical borehole images. From these image logs scanning borehole wells, preferential fracture orientation was identified among the sub-vertical fractures to be aligned along the NNW direction.

At each well, water level and temperature monitoring data were collected every 15 minutes since 2015. From these data, snowmelt infiltration appeared to dominate bedrock recharge during the spring time, while recharge from rainfall infiltration later in the season was negligible. This is likely due to high evapotranspiration and low soil moisture content above the saturated zone during the summer and fall dry seasons, which reduce bedrock recharge. To assess aquifer parameters and yield, a series of slug tests and pumping tests were conducted. The slug tests were described in detail in Ren et al. (2018), which indicated a heterogeneous distribution of vertically averaged horizontal Kh at the individual well locations. However, due to the short duration and small hydraulic forcing of the slug tests, inter-well connectivity, which controls groundwater flow in fractures at the well field scale, cannot be delineated. In this paper, we present the results of several longer duration cross-hole pumping tests, which were used to quantify not only the average Kh and Ss values surrounding the pumping boreholes, but were also interpreted using transient HT to quantify their spatial variation in an attempt to image the main fracture zones in the field. It is of interest to note that groundwater discharged during the well tests was analyzed for pH (7.5~8.0), total dissolved solids (80~188 ppm), and total suspended sediments (<4.0~51.0 ppm). Water chemistry data from the field suggest a meteoric origin of the bedrock groundwater, with snowmelt as the most likely source.

3. CROSS-HOLE PUMPING TESTS AND 2D HYDRAULIC TOMOGRAPHY

3.1 Sequential pumping tests

During the summer and winter seasons of 2015 to 2017, a total of five cross-hole pumping tests was conducted at the Blair Wallis well field:

1. The first test was performed at BW4 which lasted 28 hours from 11/18/2015 to 11/19/2015. During this test, pumping rate varied from 23 to 13 gallon per minute (gpm) due to flowing debris that damaged the submersible pump. A constant pumping rate was thus not maintained. BW1 was monitored during this test, and no drawdown was monitored in this well.

2. The second test was performed at BW7, which lasted 44 hours from 8/22/2017-8/24/2017, with a pumping rate of ~4.0 gpm. BW1, BW4, BW6, BW8, and BW9 were monitored at the same time.

3. The third test was performed at BW8 on 10/04/2017, which lasted 95 minutes with a pumping rate of ~3.0 gpm. BW1, BW4, BW6, BW7, and BW9 were monitored at the same time.

4. The fourth test was performed at BW1 on 10/25/2017, which lasted 35 minutes with a pumping rate of ~7 gpm. BW4, BW6, BW7, BW8, and BW9 were monitored at the same time.

5. The fifth test was performed at BW6 on 11/16/2017, which lasted 245 minutes with a pumping rate of ~5gpm. BW1, BW4, BW7, BW8, and BW9 were monitored at the same time.

At the well field, soil evaporation is high in the summer and fall seasons resulting in negligible bedrock recharge. During winter, the site and nearby drainage areas are covered by snow, which does not melt until early spring (April to June). Therefore, the pumping tests were conducted during summer to early winter when recharge to the aquifer is negligible, which is considered ideal for well test interpretation. The recharge flux to the aquifer, as a boundary condition, is unknown and is difficult to estimate from limited well data. During a pumping test, we pumped a chosen borehole at a near-constant rate while measuring changes in water levels at the pumping and monitoring wells using both In-Situ pressure transducers and e-tapes. During the test, a transducer was placed just above the pump at the pumping well, and for the monitoring wells, the transducers were placed sufficiently deep below the initial water level at the start of the test. All the transducers were set to record the water level changes every minute. For BW8 and BW9, static sensor noise was recorded by the transducers during the BW7 pumping test. A 15-point centrally weighted moving average method was applied to smooth the data before being used for parameter estimation.

Due to the short duration of the BW1 test, no cross-hole drawdown responses were observed at the other monitoring wells. Thus, in the following section, this test will not be included in the HT inversion analysis. Results of the 28-hour pumping test conducted at BW4 in November 2015 were included for the HT analysis. However, boreholes BW6, BW7, BW8, and BW9 had not been drilled at that time and only BW1, which showed no drawdown response to this test, was monitored. From the water level monitoring data of BW4, there was no drawdown response in this well during the pumping tests of BW1, BW6, BW7, and BW8 as well. We conjectured that there must exist a low permeability barrier between BW4 and the rest of the well field, which is consistent with the known geology and lineaments mapped in the region. Because no cross-hole drawdown was recorded during the BW1 and BW4 pumping tests, which is necessary for accurate storativity estimation, both tests were not analyzed using the well test analytical solutions.

Drawdown responses at the monitoring wells during a pumping test were displayed in Figure 2. For a given test, drawdown s is normalized by the average pumping rate Q while the elapsed time t is normalized by the squared distance between the pumping well and the monitoring well, r^2. The normalized s is plotted on the linear scale and the normalized t is plotted on the logarithm scale. These

hydrographs can provide qualitative information about fracture connectivity and flow barriers among the wells. Figure 2a shows the hydrographs at monitoring boreholes BW1, BW6, BW8, and BW9 during the pumping test of BW7. Water level at borehole BW9 responded first; BW6 and BW8 then followed; BW1 showed almost no response throughout this test. The rapid response at BW9 suggests that BW9 is connected with BW7 (likely through fractures), while a barrier likely exists between BW1 and BW7. When pumping BW8, BW7 showed the fastest response followed by BW9, while BW1 and BW6 showed little response (Figure 2b). This indicates that flow barriers likely exist between BW8 and BW1 and BW8 and BW6. During the pumping test of BW6, BW7 and BW1 showed responses at nearly the same time, followed by BW8 and BW9 (Figure 2c). This suggests that comparing to BW8 and BW9, BW1 and BW7 are more connected to BW6. These differential responses will be interpreted jointly using transient HT to image the distribution of Kh and Ss at the well field.

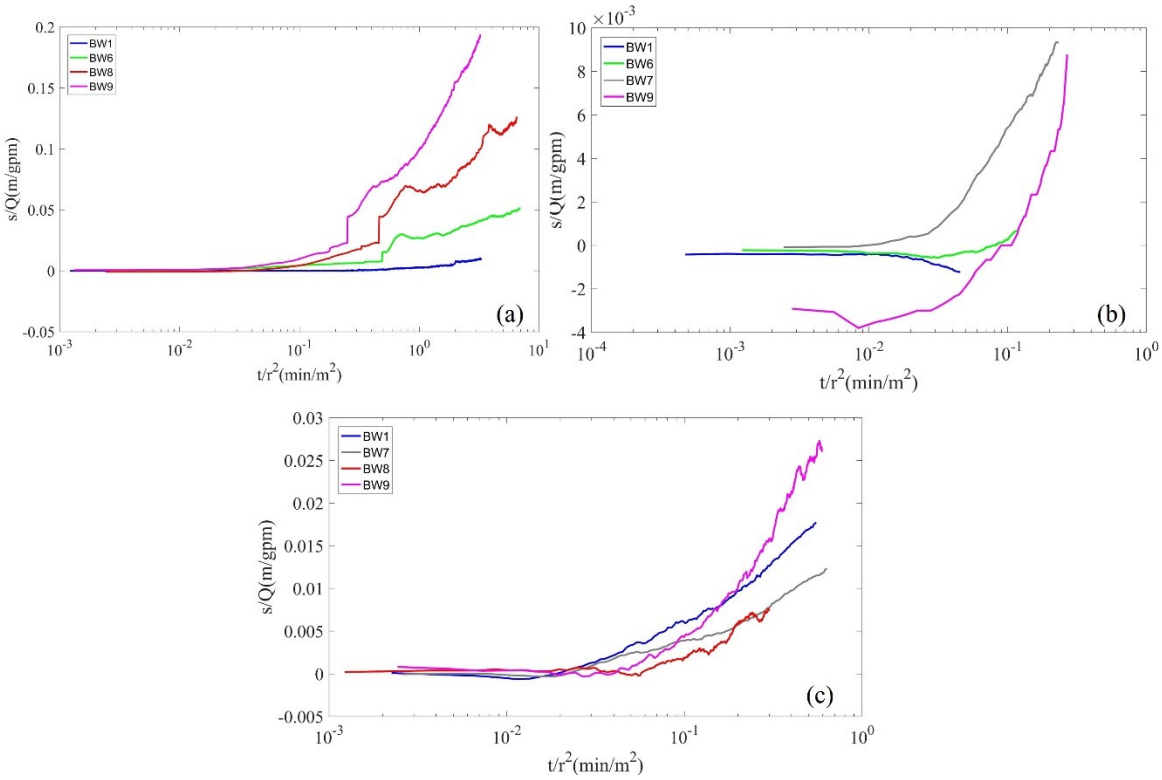

Figure 2 (a–c) Normalized drawdown versus normalized elapsed time during the pumping test of BW7, BW8, and BW6, respectively. Q is the average pumping rate and r is the distance between pumping well and a given monitoring well.

3.2 Estimation of large scale parameters using analytical solutions

From drawdown data collected during a pumping test, a large-scale Kh can be obtained using suitable analytical solutions assuming an equivalent homogeneous and infinite aquifer without leakage and recharge during the well test. While Kh can be estimated using drawdown data from the pumping well, accurate estimation of Ss, which is related to water and rock compressibilities, requires cross-hole drawdown responses. In addition, hydraulic head inferred from the transducer measurements inside the pumping well may not reflect the actual head in the aquifer outside the well due to, e.g., skin effect, wellbore storage, turbulent flow (Weight, 2008). Therefore, for a given well test, the large-scale Kh and Ss were estimated using drawdown data from the monitoring wells only. Moreover, for the 5 pumping tests described above, water level monitoring data before and after the tests do not suggest significant external recharge during the test.

The large-scale hydraulic parameters were estimated using four analytical well test solutions for an unconfined aquifer (i.e., Theis, 1935; Cooper and Jacob, 1946; Neuman, 1974; Moench, 1997). Figure 3 displayed the fitting results of pumping BW8, whereas the drawdown data interpreted by these solutions came from borehole BW7. From the curve-fitting exercise, both aquifer transmissibility (T) and storativity (S) can be obtained, which reflect average values between the pumping well and the specific monitoring well. Then, Kh and Ss were obtained by dividing T and S with the saturated thickness of the aquifer at the pumping borehole: Kh =T/L, Ss=S/L, where L is the saturated thickness. L is ~ 63m for BW8 and varies for the other wells. Three results have been derived from the curve-fitting exercise:

1, For a given pumping well, Kh estimated using different analytical solutions varies by up to 1.5 when different monitoring well drawdown was interpreted. This suggests that the different assumptions employed in these solutions did not significantly impact well test interpretation at this site.

2, The estimated Kh exhibits variable anisotropy in the horizontal direction, which suggests that fracture permeability and connectivity between a pumping well and a monitoring well varies. Using Kh interpreted from the Theis solution as an example, the approximate anisotropy ratio varies from 1.4 for BW8, to 2.7 for BW7, to 3.0 for BW6. From all four analytical solutions, relatively low values of Kh are identified between BW6-BW8 and BW6-BW9 well pairs when compared to Kh between BW6-BW7 and BW6-BW1 well pairs. This is consistent with the NNW sub-vertical fractures identified in the borehole image logs. The reason for the existence of this flow barrier is likely due to clay-rich fracture fillings: pumping and airlift tests conducted on BW6 and BW7 have removed clay and small granite minerals that have settled in the borehole in between tests.

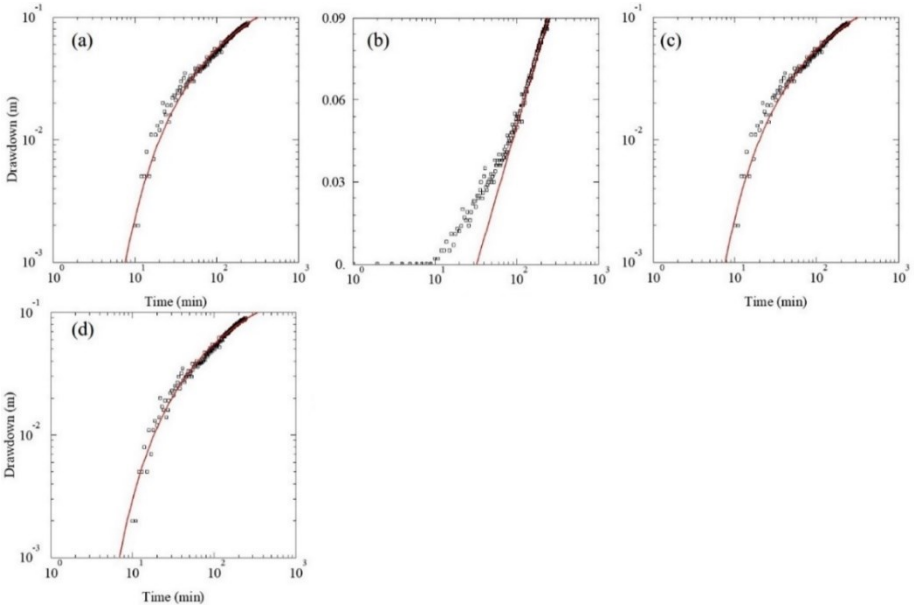

Figure 3. Curve fitting for the drawdown data collected in BW7 when BW8 was being pumped: (a) Theis (1935) solution, (b) Cooper and Jacob (1946) model, (c) Neuman (1974) model, (d) Moench (1997) model. Red solid lines indicate the best fit model and the squares indicate the drawdown from the monitoring well.

3, When compared to slug-test-derived Kh (Ren et al., 2018), pumping-test-derived Kh is ~2 orders of magnitude greater than slug-test-derived Kh at BW8, and is ~1 order of magnitude greater than slug-test-derived Kh at BW6. This is likely due to different aquifer volumes being stressed between slug test and pumping test. The "scale effect" of hydraulic conductivity is well-known when conducting well tests in fractured rocks (e.g., Hsieh, 1998; Rovey and Niemann, 2001; Hyun et al., 2002; Neuman and Di Federico, 2003; Illman, 2006). Due to the same reason, pumping-test-derived Kh for fractured rocks is likely time dependent as a longer duration test can stress a greater volume of the aquifer (Gorelick et al., 1996). Depending on whether the stressed volume reaches the representative elementary volume (REV) for the fractured medium (Bear, 1972), pumping-test-derived Kh may or may not represent the field-wide average value of this parameter. Neuman (1987) also pointed out that it may be impossible to define a REV for a typical fractured rock due to the high degree of fracture heterogeneity. In this study, we named the pumping-test-derived Kh as "large scale" Kh, acknowledging that this parameter is likely scale dependent.

3.3 Analysis of sequential pumping tests using HT

3.3.1 Successive linear estimator (SLE)

The SLE is a successive Bayesian linear estimator that derives the mean parameter fields conditioned on available spatiotemporal measurements of aquifer responses assuming prior knowledge of the mean value and spatial structures (i.e. spatial covariance functions) of the estimated parameters (Yeh et al., 1995, 1996). Unlike the above analysis using analytical solutions assuming an (equivalent) homogeneous aquifer, SLE adopts a highly parameterized heterogeneous conceptual model. As such, the problem domain for the study was discretized into N elements. SLE estimates the most likely parameter value (i.e., conditional expectation) for each element given the observed drawdown data from sequential pumping tests. To implement SLE, prior knowledge about the mean values of K and Ss parameter fields is required, which is stored in a *prior* parameter vector **Y** (2N×1) before the numerical inversion procedure. In the following, the SLE method is briefly described.

Suppose that during a single pumping test, x observed heads, denoted by a data vector **h***, have been collected at different times and at different well locations. Given these observations, the estimated parameter fields are stored in $\hat{\mathbf{Y}}$c (subscript c denotes conditional), which is iteratively determined using the following stochastic linear estimator:

$$\hat{\mathrm{Y}}_c^{(r+1)} = \hat{\mathrm{Y}}_c^{(r)} + \omega^{\mathrm{T}}\left(\mathbf{h}^* - \mathbf{h}^{(r)}\right) \qquad (1)$$

where superscript r is iteration index; superscript T denotes the transpose; $\mathbf{h}^{(r)}$ are simulated heads at the observation locations and times obtained from a numerical forward model using the parameter fields obtained at iteration r. Note that when r=0, $\hat{\mathbf{Y}}\mathbf{c} = \mathbf{Y}$ (the prior). The coefficient matrix ω (x×2N) denotes a set of weights, which assign the contribution of the difference between the observed and simulated head at each observation location and time to the previously estimated parameter value at each element. The weight matrix ω is determined by solving the following equation which requires the knowledge of covariance ε_{hh} and cross-covariance ε_{hy} at each iteration:

$$\left[\varepsilon_{hh}^{(r)} + \theta^{(r)} diag\left(\varepsilon_{hh}^{(r)}\right)\right]\omega^{(r)} = \varepsilon_{hy}^{(r)} \qquad (2)$$

where ε_{hh} is covariance matrix of the observations (or data), ε_{hy} is cross-covariance matrix between parameters and data, θ is a dynamic stability multiplier, and diag(ε_{hh}) is a stability matrix, which is a diagonal matrix with the same diagonal entries as ε_{hh}. Both the covariance and cross-covariance matrices can be calculated using first-order numerical approximation (Yeh and Liu, 2000):

$$\varepsilon_{hh}^{(r)} = \mathrm{J}_h^{(r)}\varepsilon_{yy}^{(r)}\mathrm{J}_h^{(r)\mathrm{T}}, \quad \varepsilon_{hy}^{(r)} = \mathrm{J}_h^{(r)}\varepsilon_{yy}^{(r)} \qquad (3)$$

where $\mathrm{J}_h^{(r)}$ (x×2N) is the sensitivity (Jacobian) matrix of head data with respect to the element-wise parameters using the parameters estimated at iteration r; $\varepsilon_{yy}^{(r)}$ (2N×2N without compressed storage) is the parameter covariance matrix at iteration r. At iteration r=0, ε_{yy} is the unconditional covariance of the parameters constructed from the assumed geologic structures of lnK and lnSs, i.e., variance, covariance function, correlation scales. For r≥1, ε_{yy} becomes a conditional covariance matrix which can be evaluated according to:

$$\varepsilon_{yy}^{(r+1)} = \varepsilon_{yy}^{(r)} - \omega^{\mathrm{T}}\varepsilon_{hy}^{(r)} \qquad (4)$$

Equations (1) to (4) describe the SLE algorithm using data from a single pumping test. Based on this algorithm, data from several pumping tests can be assimilated conjunctively by adopting one of two approaches, e.g., Sequential SLE (SSLE) or Simultaneous SLE (SimSLE) (Zhu and Yeh, 2005; Xiang et al., 2009). Either approach, with detail on its implementation described in the above references, constitutes the core of the hydraulic tomography technique.

3.3.2 Two-dimensional HT analysis of sequential pumping tests

For the Blair Wallis field site, we analyzed the four pumping tests using the SimSLE algorithm of Xiang et al. (2009). Because the bedrock wells are open holes below the casing, and packer system is not installed in these boreholes, only a 2D HT analysis along the horizontal plane can be performed. For this analysis, the model domain is 160×80m and is discretized into 80×40 uniform square cells (each cell is of size 2×2m) (Figure 4). During inversion, the forward model simulated each transient pumping test using Variably Saturated Flow and Transport in 2D (VSAFT2), a finite element code developed by Yeh et al. (1993). Initial conditions for the forward model were set by assuming that groundwater was hydrostatic at the start of each pumping test. During the simulation, constant head boundary conditions were assigned to the west and east boundaries, while the north and south were assumed no-flux boundaries. Recharge to the model was consider negligible during the simulation. Each pumping test was simulated using the flow rate (constant or temporally variable) measured in the field. Thus, the source/sink strength for each pumping test was assumed fully known during inversion.

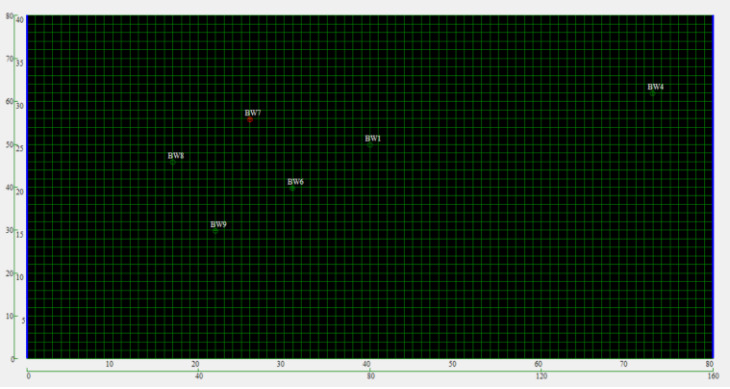

Figure 4 Finite element grid of the forward model with 3321 nodes and 3200 elements. The model domain incorporates the 6-well cluster: BW1, 4, 6, 7, 8, 9.

In SimSLE, the mean K and Ss fields as well as their correlation scales are assumed to be known prior to inversion. In this work, inversion was initialized with homogeneous mean fields of K= 1.0×10-5 m/s and Ss= 1.0×10-5 m-1, which were assigned using average values obtained from interpreting the pumping tests with analytical solutions (Sec. 3.2). Exponential correlation functions were assumed to describe the unconditional spatial structures of K and Ss, and the correlation scales were set to 15 m for both parameters and along both x and y directions. The variances of lnK and lnSs were set to 5.0 and 2.0, respectively. The inversion starts with a cokriging step using all available measurements of hydraulic properties and hydraulic heads to produce the conditional parameter fields at r=0. The

stochastic conditional means of these parameters were then used by the forward model to predict heads at selected observation locations and times. The cokriged parameter fields of lnK and lnSs were then iteratively updated by SimSLE to minimize the differences between the observed and the simulated heads.

According to Sun et al. (2013), drawdown of a monitoring well at the interpolated time at which drawdown is zero in the Cooper–Jacob log-linear model is the most correlated with Ss over a large portion of the aquifer, while late-time drawdown at the same monitoring well is highly correlated to Kh over the entire aquifer. For estimating Ss using SimSLE, Yeh et al. (2011) and Mao et al. (2013) emphasized that head change over at least two iteration steps is necessary to determine Ss. Because drawdown at a monitoring well during a pumping test is highly correlated in time, Zhu and Yeh (2005) suggested that 4 to 5 points sampled from the hydrograph of the observed drawdown at a monitoring well are sufficient to condition the inversion. This also significantly reduces the computational burden of the inversion, as the forward model must be repeatedly run during each iteration. In this study, following this recommendation, the observed heads were sampled from the monitored drawdown data (collected at 1 min intervals) sparingly, but included both early- and late time data. An example showing the sampling points along with the observed and simulated drawdown data for the pumping test of BW7 is shown (Figure 5). For this test, four heads were selected from BW1's hydrograph, twelve heads were selected from BW6's hydrograph, eleven heads were selected from BW8's hydrograph, and nine heads were selected from BW9's hydrograph. For the pumping tests of BW8 and BW6, however, four heads were sampled from the hydrograph of each monitoring well. This was found to yield satisfactory results without invoking unduly high number of iterations.

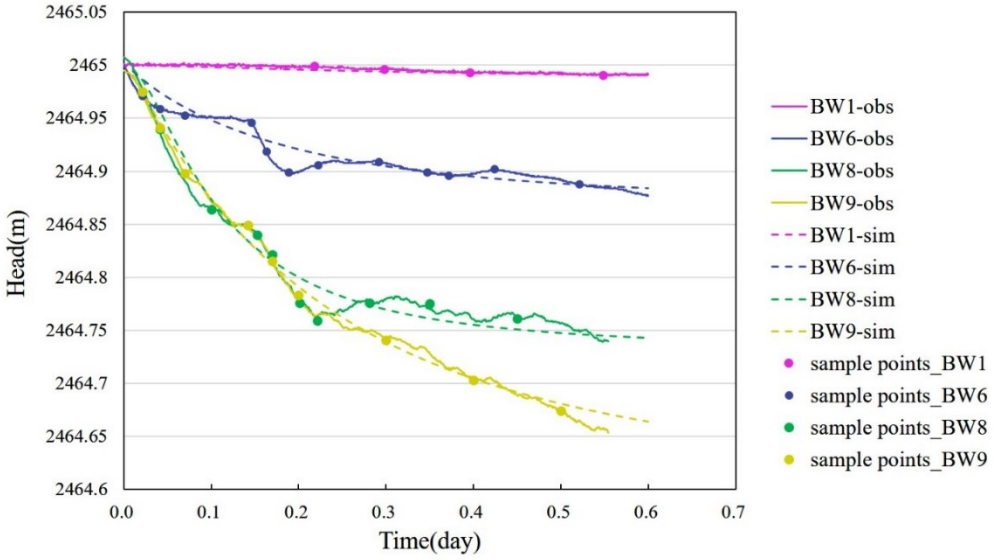

Figure 5 Hydrographs show the sampling points along with the observed and simulated drawdown in monitoring wells when BW7 was pumped.

Using SimSLE, the estimated Kh and Ss fields after assimilating four pumping tests (i.e., BW7, 8, 6, and 4 pumping tests) are shown in Figure 6. In Figure 6a, the analysis yielded the highest K zone between BW7 and BW9 and another high K zone between BW7 and BW8. There is a flow barrier between BW7 and BW1. A barrier also exists between BW4 and the rest of the wells. Although there are low K zones between BW8 and BW9, BW6 and BW7, as well as between BW6 and BW9, these wells are still connected. Generally, the inverted Kh field is consistent with the observed drawdown data (Figure 2). However, two abnormal high K zones are observed near the left and right boundaries. We attribute this to boundary effect, since the boundary conditions assigned to the forward model were assumed values.

The estimated Ss tomogram indicates that BW7, BW6, BW9 are well interconnected (Figure 6b). The Ss tomogram is negatively correlated with the corresponding Kh tomogram, while its estimated value is generally lower at the boreholes with rapid responses. Both the estimated K and Ss tomograms are plausible because they can explain the *largest* observed drawdown behaviors: (1) BW9 recorded large and rapid responses during the pumping test of BW7; (2) BW7 recorded rapid responses during the pumping of BW8; (3) BW7 recorded rapid responses during the pumping of BW6. The simulated heads versus the observed heads were then compared directly (Figure 7). A linear model was fitted to the scatter plot without forcing the intercept to zero. As shown by the fitting statistics, the simulated heads and the observed heads are in good agreement, suggesting that the inversion results are adequate.

To quantitatively assess the estimation errors, a conditional L2 norm of the heads can be computed at the end of each iteration during the inversion (Xiang et al. 2009):

$$L2^{(r)} = \frac{1}{m}\sum_{i=1}^{m}(h_i^* - \hat{h}_i^{(r)})^2 \qquad (5)$$

where h_i^* and $\hat{h}_i^{(r)}$ are observed and simulated heads at the r^{th} iteration, respectively; i is the numbering index for the observations; m is the total number of head observations used in inversion. Figure 8 shows the conditional L2 norm versus the number of iterations during the joint inversion of the four pumping tests. L2 norm decreases with increasing iterations and stabilizes after iteration 15. At this point, variances of the estimated lnKh and lnSs fields also stabilized within a user-supplied tolerance level, thus the iteration was terminated. By jointly using the L2 norm with the parameter variances as a convergence criterion, overexploitation of noisy data is avoided.

For the SimSLE analysis assimilating 4 pumping tests at the Blair Wallis well field, estimation variances of lnK and lnSs were also computed (Xiang et al. 2009). Uncertainty in the estimated Kh and Ss is generally lower in the region near the pumped and observation locations, as expected (Figure 9). The uncertainty grows larger away from the observation locations, and becomes the largest near the model boundaries. This is also expected given that no observations were available along these boundaries. Overall, uncertainty of both parameters in the area enclosed by BW1, BW6, BW7, BW8, and BW9 is the smallest. Therefore, fractures connectivity and permeability at the well field can only be reliably inferred in the inter-well region.

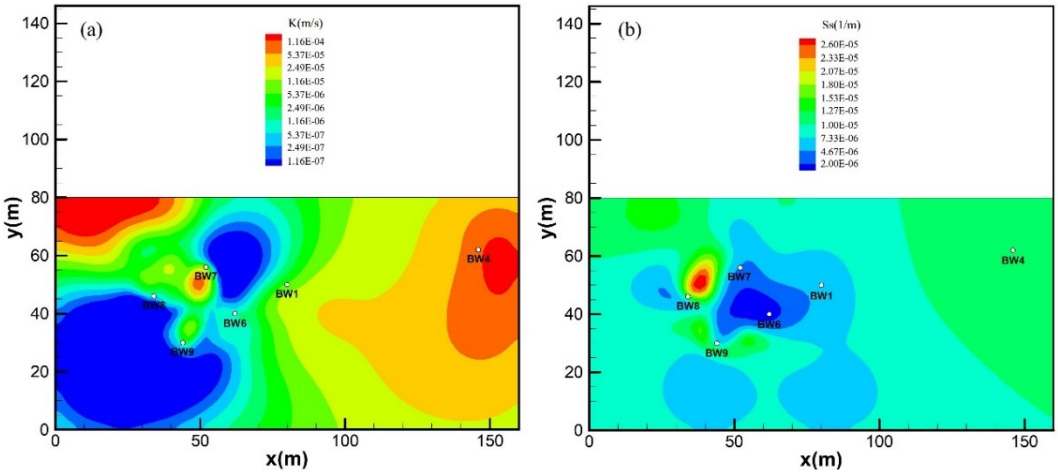

Figure 6 Inverted Kh (a) and Ss (b) tomograms from joint inversion of four pumping tests (BW7, 8, 6, and 4).

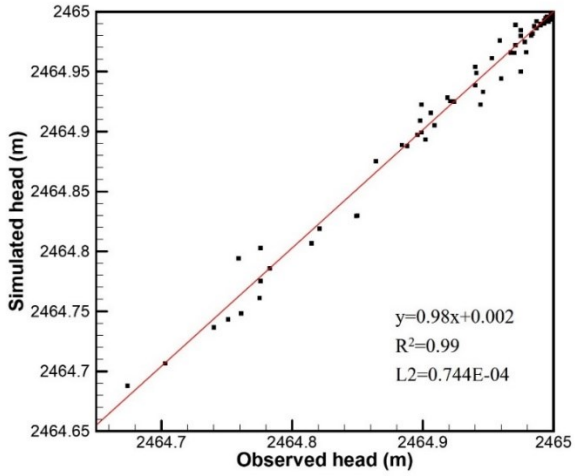

Figure 7 Simulated versus observed heads after jointly inverting the four pumping tests.

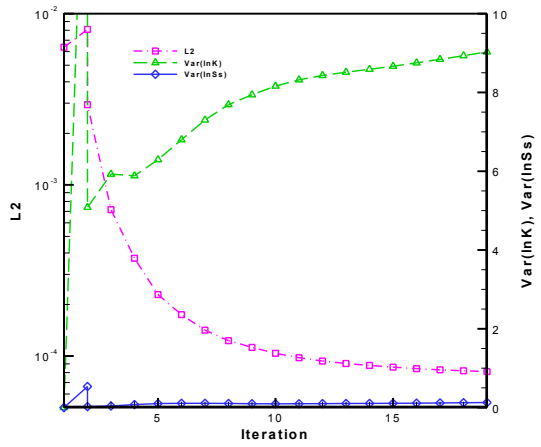

Figure 8 Conditional L2 norm of hydraulic head, Var(lnK), and Var(lnSs) versus the number of iterations during the simultaneous inversion of the four pumping tests.

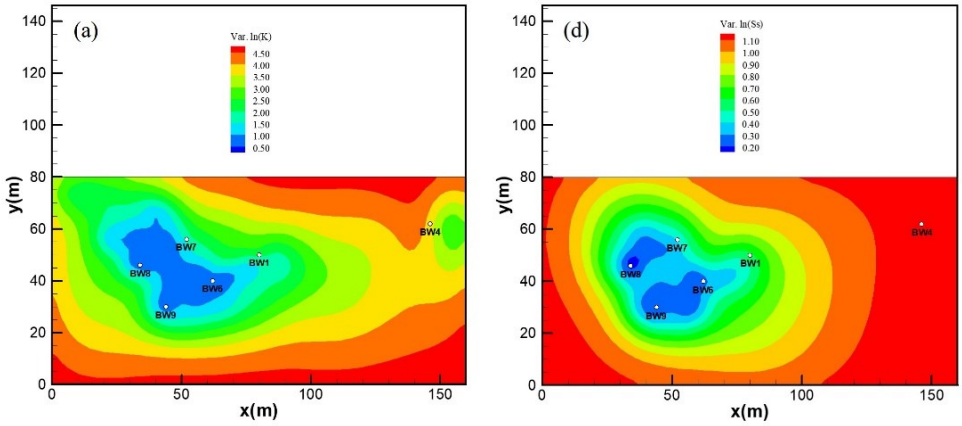

Figure 9 Estimation variances of lnKh (a) and lnSs (b) for the inversion of four cross-hole pumping tests.

4. CONCLUSIONS

Hydraulic properties of a fractured granite aquifer in the Laramie Range, Wyoming, were investigated using cross-hole pumping tests among 6 bedrock boreholes. Results of four cross-hole pumping tests were interpreted using analytical solutions as well as using SimSLE, a two-dimensional transient hydraulic tomography (HT) algorithm. Our results are summarized in the following:

(1) The average K_h and Ss derived from pumping test analysis using analytical solutions is on the order of 10^{-5}m/s and 10^{-4} m^{-1}, respectively. The estimated K_h and Ss from all five models (i.e., Theis (1935) model, Cooper and Jacob (1946) model, Neuman (1974) model, Moench (1997) model) are close despite the difference in the assumptions of these models.

(2) HT is a useful technique for imaging inter-well permeability heterogeneity. The SimSLE algorithm was able to image continuous high K_h and low specific storage (Ss) zones among the boreholes. These zones thus have high hydraulic diffusivity (K_h/Ss), which suggests fast groundwater flow in preferential pathways which likely reflect connected open fractures. In addition, SimSLE identified a low K_h barrier between BW4 and the rest of the wells, which is consistent with what is known from the site geological, drilling, and geophysical data.

(3) Scale effect is observed as the pumping-test-inferred K_h is more than a factor of 5 greater than the slug-test-inferred Kh for several boreholes, suggesting fractures with greater permeability were encountered when the well test volume was expanded.

5. FUTURE WORK

Hydraulic tomography can be used to estimate aquifer flow parameters with greater spatial resolution than class well test interpretation techniques. However, at the Blair Wallis well field, fracture networks cannot be resolved for the individual fractures given the number of available pumping tests conducted. Greater resolution of the parameters requires increased spatial measurement density (i.e., number of wells), which can be impractical. Drilling more wells can also change the hydraulics of the aquifer system because wells have different permeability and storativity than the in-situ aquifer parameters. Future work will investigate approaches to improve resolutions without requiring greater spatial measurement density. In particular, we aim to explore HT approaches that can take advantage of both

drawdown and downhole high-resolution flowmeter logging data for parameter estimation. Flowmeter logging, at its current stage, can identify inflows and outflows from individual fractures as well as their variation in magnitude and direction induced by pumping and also later, during recovery. Future work will also investigate borehole instrumentation with multilevel hydraulic head monitoring systems, thus hydraulic conductivity and Ss heterogeneity may be imaged in three dimensions.

REFERENCES

Bear, J., 1972. Dynamics of Fluids in Porous Media [M]. New York: American Elsevier Publishing Co.

Berg S J, Illman W A., 2013. Characterization of hydraulic conductivity heterogeneity with steady state hydraulic tomography: Field study in a highly heterogeneous glaciofluvial deposit. Ground Water, 51(1): 29-40.

Bradley W C., 1987. Erosion surfaces of the Colorado Front Range: a review. Geomorphic systems of North America. Centennial Spec, 2: 215-220.

Brauchler R, Liedl R, Dietrich P., 2003. A travel time based hydraulic tomographic approach. Water Resources Research, 39(12).

Cardiff M, Barrash W, Kitanidis P K., 2012. A field proof- of- concept of aquifer imaging using 3D transient hydraulic tomography with modular, temporarily- emplaced equipment. Water Resources Research, 48(5).

Castagna M, Bellin A., 2009. A Bayesian approach for inversion of hydraulic tomographic data. Water Resources Research, 45(4).

Castagna M, Becker M W, Bellin A., 2011. Joint estimation of transmissivity and storativity in a bedrock fracture. Water Resources Research, 47(9).

Chapin C E, Kelley S A., 1997. The Rocky Mountain erosion surface in the Front Range of Colorado.

Cooper H H, Jacob C E., 1946. A generalized graphical method for evaluating formation constants and summarizing well- field history. Eos, Transactions American Geophysical Union, 27(4): 526-534.

Edwards B R, Frost C D., 2000. An overview of the petrology and geochemistry of the Sherman batholith, southeastern Wyoming Identifying multiple sources of Mesoproterozoic magmatism. Rocky Mountain Geology, 35(1): 113-137.

Eggler D H, Larson E E, Bradley W C., 1969. Granites, grusses, and the Sherman erosion surface, southern Laramie Range, Colorado-Wyoming. American Journal of Science, 267(4): 510-522.

Evanoff E., 1990. Early Oligocene paleovalleys in southern and central Wyoming: Evidence of high local relief on the late Eocene unconformity. Geology, 18(5): 443-446.

Flinchum B A, Steven Holbrook W, Rempe D, et al., 2018. Critical zone structure under a granite ridge inferred from drilling and three- dimensional seismic refraction data. Journal of Geophysical Research: Earth Surface, 123(6): 1317-1343.

Frost C D, Frost B R, Chamberlain K R, et al., 1999. Petrogenesis of the 1.43 Ga Sherman batholith, SE Wyoming, USA: a reduced, rapakivi-type anorogenic granite. Journal of Petrology, 40(12): 1771-1802.

Geist D J, Frost C D, Kolker A, et al., 1989. A geochemical study of magmatism across a major terrane boundary: Sr and Nd isotopes in Proterozoic granitoids of the southern Laramie Range, Wyoming. The Journal of Geology, 97(3): 331-342.

Gregory K M, Chase C G., 1994. Tectonic and climatic significance of a late Eocene low- relief, high- level geomorphic surface, Colorado. Journal of Geophysical Research: Solid Earth, 99(B10): 20141-20160.

Hao Y, Yeh T C J, Xiang J, et al., 2008. Hydraulic tomography for detecting fracture zone connectivity. Groundwater, 46(2): 183-192.

Hsieh P A., 1998. Scale effects in fluid flow through fractured geologic media. In: Sposito, G. (Ed.), Scale Dependence and Scale Invariance in Hydrology. Cambridge University Press, Cambridge, pp. 335–353.

Hyun Y, Neuman S P, Vesselinov V V, et al., 2002. Theoretical interpretation of a pronounced permeability scale effect in unsaturated fractured tuff. Water Resources Research, 38(6).

Illman W A., 2006. Strong field evidence of directional permeability scale effect in fractured rock. Journal of Hydrology, , 319(1-4): 227-236.

Illman W A, Liu X, Takeuchi S, et al., 2009. Hydraulic tomography in fractured granite: Mizunami Underground Research site, Japan. Water resources research, 45(1).

Illman, W.A., 2014. Hydraulic Tomography Offers Improved Imaging of Heterogeneity in Fractured Rocks. Groundwater, 52(5): 659-684.

A. Jardani, A. Revil, J.P. Dupont (2013) Stochastic joint inversion of hydrogeophysical data for salt tracer test monitoring and hydraulic conductivity imaging, Advances in Water Resources, Volume 52: 62-77.

Johnson, R.C., and F.A. Hills., 1976. Precambrian geochronology and geology of the boxelder canyon area, northern Laramie range, Wyoming. Geological Society of America Bulletin 87(5): 809–817.

Krásný Jirí and John M. Sharp, 2003. Groundwater in Fractured Rocks: IAH Selected Paper Series, volume 9 (IAH - Selected Papers on Hydrogeology) 1st Edition.

Liu S, Yeh T C J, Gardiner R., 2002. Effectiveness of hydraulic tomography: Sandbox experiments. Water Resources Research, 38(4): 5-1-5-9.

Liu X, Kitanidis P K., 2011. Large- scale inverse modeling with an application in hydraulic tomography. Water Resources Research, 47(2): W02501.

Mao D, Yeh T C J, Wan L, et al., 2013. Necessary conditions for inverse modeling of flow through variably saturated porous media. Advances in water resources, 52: 50-61.

Matsuki, K., Chida, Y., Sakaguchi, K., Glover, P.W.J., 2006. Size effect on aperture and permeability of a fracture as estimated in large synthetic fractures. Int. J. RockMech. Min. 43, 726–755.

Mears Jr B., 1993. Geomorphic history of Wyoming and high-level erosions surfaces. In A. W. Snoke, J. R. Steidtmann, & S. M. Roberts (Eds.), Geology of Wyoming. Cheyenne, Wyoming: Wyoming Geological Survey, 5: 608–626.

Meier P M, Medina A, Carrera J., 2001. Geostatistical inversion of cross- hole pumping tests for identifying preferential flow channels within a shear zone. Groundwater, 39(1): 10-17.

Moench A F., 1984. Double- porosity models for a fissured groundwater reservoir with fracture skin. Water Resources Research, 20(7): 831-846.

Moore, F. E., 1960. Summary of Cenozoic history, southern Laramie Range, Wyoming and Colorado. In R. J. Weimer and J. D. Haun (Eds.), Guide to the geology of Colorado. Denver, CO: Rocky Mountain Association of Geologists: 217–222.

National Resources Conservation Service., 2015. Crow Creek SNOTEL site, United States Department of Agriculture, SNOTEL surveys. Available online at http://wcc.sc.egov.usda.gov/nwcc/site?sitenum=1045

Neuman S P., 1974. Effect of partial penetration on flow in unconfined aquifers considering delayed gravity response. Water resources research, 10(2): 303-312.

Neuman, S.P., 1987. Stochastic continuum representation of fractured rock permeability as an alternative to the REV and fracture network concepts. In Rock Mechanics: Proceedings of the 28th US Symposium, Tucson, AZ, eds. I.W. Farmer, J.J.K. Daemen, C.S. Desai, C.E. Glass, and S.P. Neuman: 533–561..

Neuman S P, Di Federico V., 2003. Multifaceted nature of hydrogeologic scaling and its interpretation. Reviews of Geophysics, 41(3).

Odonne, F., Lézin, C., Massonnat, G., Escadeillas, G., 2007. The relationship between joint aperture, spacing distribution, vertical dimension and carbonate stratification: an example from the Kimmeridgian limestones of Pointe-du-Chay (France). J. Struct. Geol. 29, 746–758.

Peterman Z E, Hedge C E., 1968. Chronology of Precambrian events in the Front Range, Colorado [J]. Canadian Journal of Earth Sciences, 5(3): 749-756.

Ren, S., Gragg, S., Zhang, Y., Carr, B., Yao, G., 2018. Borehole characterization of hydraulic properties and groundwater flow in a crystalline fractured aquifer of a headwater mountain watershed, Laramie Range, Wyoming. J. Hydrol. 561, 780–795.

Rovey II C W, Niemann W L., 2001. Wellskins and slug tests: where's the bias?. Journal of Hydrology, 243(1-2): 120-132.

Schöniger A, Nowak W, Hendricks Franssen H J., 2012. Parameter estimation by ensemble Kalman filters with transformed data: Approach and application to hydraulic tomography. Water Resources Research, 48(4).

Scott G R, Taylor R B., 1986. Map Showing Late Eocene Erosion Surface, Oligocene-Miocene Paleovalleys, and Tertiary Deposits in the Pueblo, Denver, and Greeley 1°x 2°quadrangles, Colorado. US Geological Survey.

Snodgrass M F, Kitanidis P K., 1998. Transmissivity identification through multi-directional aquifer stimulation. Stochastic Hydrology and Hydraulics, 12(5): 299-316.

Sharmeen R, Illman W A, Berg S J, et al., 2012. Transient hydraulic tomography in a fractured dolostone: Laboratory rock block experiments. Water Resources Research, 48(10).

Sun R, Yeh T C J, Mao D, et al., 2013. A temporal sampling strategy for hydraulic tomography analysis. Water Resources Research, 49(7): 3881-3896.

Theis C V., 1935. The relation between the lowering of the piezometric surface and the rate and duration of discharge of a well using ground- water storage. Eos, Transactions American Geophysical Union, 16(2): 519-524.

Weight W D., 2008. Hydrogeology field manual. McGraw-Hill.

Xiang J, Yeh T C J, Lee C H, et al., 2009. A simultaneous successive linear estimator and a guide for hydraulic tomography analysis. Water Resources Research, 45(2).

Yeh T C J, Srivastava R, Guzman A, et al., 1993. A numerical model for water flow and chemical transport in variably saturated porous media. Groundwater, 31(4): 634-644.

Yeh T C J, Gutjahr A L, Jin M., 1995. An iterative cokriging- like technique for ground- water flow modeling. Groundwater, 33(1): 33-41.

Yeh T C J, Jin M, Hanna S., 1996. An iterative stochastic inverse method: Conditional effective transmissivity and hydraulic head fields. Water Resources Research, 32(1): 85-92.

Yeh T C J, Liu S., 2000. Hydraulic tomography: Development of a new aquifer test method. Water Resources Research, 36(8): 2095-2105.

Yeh T C J, Mao D, Wan L, Lee, C H, Wen J C, Hsu K C, 2011. Well Definedness, Scale Consistency, and Resolution Issues in Groundwater Model Parameter Identification. University of Arizona, Tucosn.

Zha Y, Yeh T C J, Illman W A, et al., 2016. An application of hydraulic tomography to a large- scale fractured granite site, Mizunami, Japan. Groundwater, 54(6): 793-804.

Zhu J, Yeh T C J., 2005. Characterization of aquifer heterogeneity using transient hydraulic tomography [J]. Water Resources Research, 41(7): 1-10.

Zielinski R A, Peterman Z E, Stuckless J S, et al., 1982. The chemical and isotopic record of rock-water interaction in the Sherman Granite, Wyoming and Colorado. Contributions to Mineralogy and Petrology, 78(3): 209-219.